Astronomy & Astrophysics

Radiation pressure on dust explaining the low ionized broad emission lines in active galactic nuclei

Dust as an important driver of line shape

M. H. Naddaf[1,2] and B. Czerny[1]

[1] Center for Theoretical Physics, Polish Academy of Sciences, Lotników 32/46, 02-668 Warsaw, Poland
e-mail: naddaf@cft.edu.pl
[2] Nicolaus Copernicus Astronomical Center, Polish Academy of Sciences, Bartycka 18, 00-716 Warsaw, Poland

ABSTRACT

Context. Broad emission lines are the most characteristic features in the spectra of galaxies with an active galactic nucleus (AGN). They mostly show either single-peaked or double-peaked profiles and originate from a complex dynamics of the likely discrete clouds moving in a spatially extended region known as the broad line region (BLR).
Aims. In this paper, we present a large grid of results, which is used to test the model based on calculations of the spectral line generic profiles.
Methods. We followed a non-hydrodynamical single-cloud approach to BLR dynamics based on a radiatively dust-driven model. We previously showed in detail that the 2.5D version of the model could provide us with the 3D geometry of the BLR.
Results. We show that the shape of profiles not only depends on the accretion rate of the source, the black hole mass, and the viewing angle, but it is most significantly affected by the adopted dust-to-gas mass ratio regulating the strength of the radiation pressure. We also show that the model can aptly explain the low ionized broad emission lines of the mean spectrum of quasars, such as MgII and Hβ.
Conclusions. The radiatively dust-driving mechanism can appropriately account for the low-ionized part of BLR of AGNs.

Key words. accretion, accretion disks – radiation: dynamics – line: profiles – radiative transfer – galaxies: active – quasars: emission lines

1. Introduction

The broad line region (BLR) in active galaxies is a turbulent and spatially extended region (Wandel et al. 1999; Kaspi et al. 2000; Netzer 2020) that has not yet been fully resolved, except for a few cases of magnified BLR due to gravitational lensing (Sluse et al. 2012; Guerras et al. 2013) as well as the VLR GRAVITY observations in the IR (GRAVITY Collaboration 2018, 2020a, 2021). Hence, studies of broad emission lines stemming from this region have been based on the analysis of the spectra and their time dependence (Boroson & Green 1992; Lawrence et al. 1997; Sulentic et al. 2000; Reeves & Turner 2000; Gaskell 2009; Le & Woo 2019; Raimundo et al. 2020). However, the broad emission lines (BELs) from a BLR are a unique probe that can be used to improve our understanding of the physics of AGNs and, eventually, they can help to measure the mass of the central supermassive black hole. These emission lines are divided into two categories of high ionization lines (HIL) and low ionization lines (LIL) (Collin-Souffrin et al. 1988; Netzer 2013), and they are frequently observed in the form of single-peaked or double-peaked profiles (Osterbrock 1977, 1981; Gezari et al. 2007; Shen et al. 2011; Negrete et al. 2018; Zhang et al. 2019; Lu et al. 2021; Li et al. 2021). The shape of BELs depends on the distribution and dynamics of material within the BLR. There have been two mainstream studies that have been ongoing for years on the theoretical side to recover the observed shape of emission lines: one based on proposing

theoretically motivated mechanisms for the formation of BLR and the other one on the basis of assuming a certain distribution of material in a BLR (i.e., parametric models).

The BLR in parametric models can have different geometries of interest depending on the purpose, for example a ring, a disk, a shell, or a cone filled with clouds in which the density of clouds is assumed to follow a certain function (Netzer & Laor 1993; Ward et al. 2014; Adhikari et al. 2016, 2018; GRAVITY Collaboration 2018). As the name of these models implies, the distribution, density, and other physical properties of clouds in the BLR are parameterized in order to optimize the shape of emission lines and time-delays map (Pancoast et al. 2011, 2014; Li et al. 2013). In order to fit the data, they either infer the transfer function (Blandford & McKee 1982; Horne et al. 1991; Krolik & Done 1995; Li et al. 2016) or provide a quantitative constraints on the dynamics and geometry of BLR (Li et al. 2013; Pancoast et al. 2014). Although these models are useful, providing insights into the connection between the BLR geometry and line shape, while fiting the observational data, they are not intended to provide the theoretically motivated scenario behind the picture.

On the other hand, we previously showed that the failed radiatively accelerated dusty outflow (FRADO) model (Czerny & Hryniewicz 2011), among all other already proposed theoretical mechanisms, may effectively account for the formation and the dynamics of the LIL part of BLR such as Hβ and MgII (Naddaf et al. 2021). A preliminary test of the model
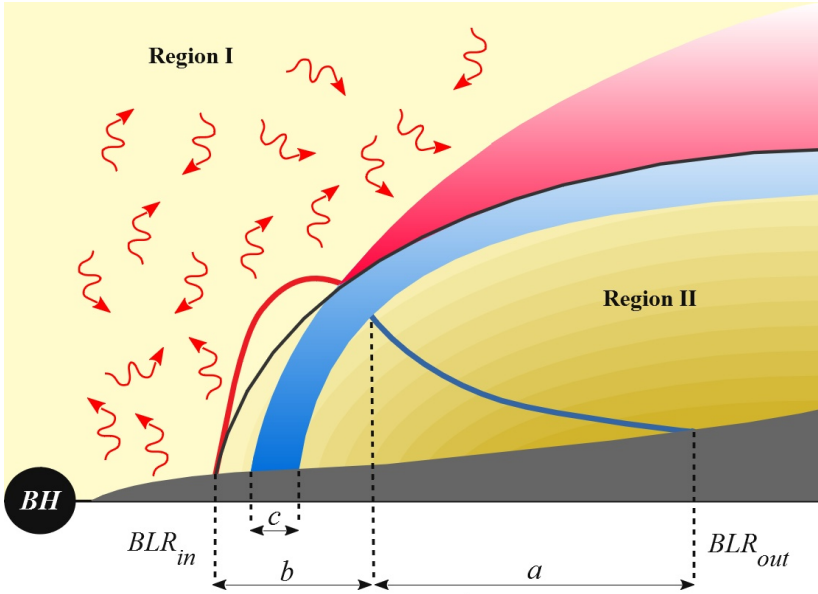
Fig. 1. Schematic illustration of BLR shape and its components in FRADO. The components of BLR are represented as (*a*) an outer tail consisting of dusty failed winds (simple up-and-down motions), (*b*) an inner region with slightly-to-broadly elongated elliptical orbits, and (*c*) a funnel-shaped outflow stream of clouds. The red and blue solid lines show the peak height of the trajectories of dustless and dusty clouds, respectively. The BLR_{in} and BLR_{out} set the two ends of a radial region of the accretion disk within which the material can be lifted due to disk radiation pressure. The black solid line represents the sublimation location. Region I marks the hot region above the sublimation location where dust cannot survive; the central disk UV radiation reaches the clouds via scattering by the hot gas in this region. Region II underneath of the sublimation location and cold enough for dust survival is obscured by the outflow stream; it prevents the BLR material from receiving the scattered ionizing radiation.

also showed that it reproduces the reverberation-known location of the LIL BLR (Peterson et al. 2004; Bentz et al. 2009, 2013) without including any arbitrary parameter; it can also successfully explain the observed dispersion in Hβ radius–luminosity (RL) relation based on the accretion rate (Naddaf et al. 2020). On the other hand, the high ionization lines such as CIV and HeII are located much closer to the center (e.g., Wandel et al. 1999; Grier et al. 2013) where dust cannot form and dust-driving mechanism is not available; thus, they are most likely to be related to line-driven winds (Proga et al. 2000; Dyda & Proga 2018) or thermally driven winds (e.g., Ganguly et al. 2021).

In this paper, we aim to test the model by calculating the line profiles. We begin by introducing a relatively large grid table of results for a range of black hole masses, accretion rates, and dust-to-gas mass ratio of clumps. We briefly explain the physics of BLR dynamics in 2.5D FRADO in Sect. 2. The numerical setup is introduced in Sect. 3. The physics of LIL BLR emission lines and the method behind the line profile calculation is addressed in the Sect. 4. We then present our results in Sect. 5, followed by a discussion in Sect. 6.

2. BLR Dynamics in 2.5D FRADO

The 2.5D FRADO model (see Naddaf et al. 2021, for full details) is a nonhydrodynamical single-cloud approach to LIL BLR dynamics. It is the enhanced version of the basic 1D model of Czerny & Hryniewicz (2011), a model based on the presence of dust in the atmosphere of an accretion disk at large radii, where it is cold enough (Rees et al. 1969; Dong et al. 2008). The FRADO model works on the basis of radiatively dust-driving mechanism, so the disk radiation pressure acting on the initially dusty material (clumps) at the surface layers of the accretion disk leads to a (mostly failed) outflow from the accretion disk. We should stress here that only dust processes do the job in this model, and the line-driving or electron scattering forces are negligible at these radii – rendering this model appropriate for studies of the LIL BLR. General relativistic effect are also negligible at these large radii, so they were neglected.

In the 2.5D FRADO, the model is enhanced with the realistic description of the dust opacities interacting with the radiation field. Geometrical configurations as proxies for the

shielding effect are necessary for launching an efficient outflow, as suggested previously by numerous authors (Shlosman et al. 1985; Voit 1992; Murray et al. 1995; Proga & Kallman 2004; Risaliti & Elvis 2010; Mizumoto et al. 2019). These are incorporated into the model in order to protect the dusty clumps from the intense central disk radiation, avoiding, hence, an overly rapid sublimation of the dust content of the clouds. Most AGNs do not show the double-peaked line profiles expected from the illuminated disk surface, so in order to produce single-peaked line profiles, the material has to reach a high vertical velocity under the continuous radiative force from below. The timescale of the process depend very much on the black hole mass, as the strong radiative force must act for a period being a noticeable fraction of the local Keplerian period. A similar requirement is necessary for line-driving winds responsible for the HIL part of the BLR, where shielding is needed in order to prevent an overionization of the medium and loss of the driving power. Clumps at initially circular local Keplerian orbits are launched (with a zero vertical velocity) from the disk surface by the disk radiation pressure and move under the radiative force from the accretion disk and gravitational field of the central black hole. The radial dependent height of the disk (disk surface) for the grid of initial conditions in our model was calculated using a separate code (Różańska et al. 1999; Czerny et al. 2016). Upon attaining high altitudes, depending on the launching radius, clumps may lose their dust content due to strong radiation from inner radii of the disk and continue their motion in the form of a free-fall in the black hole gravitational field; otherwise, they would remain dusty during the motion. Moreover, depending on the launching location clumps may escape into infinity or return to the disk surface, however, they cannot cross the disk.

The whole pattern of the trajectories of clouds depends on the initial physical parameters, and the geometry of LIL BLR in our model was determined by the kinematics of the clouds. As previously studied (Naddaf et al. 2021), it does not resemble the simple (or complicated) shapes in parametric models. We showed that the overall picture of LIL BLR can be either very complex or just as simple as an up-and-down motion, depending on the accretion rate. The general pattern of motion in FRADO consists of three components, as indicated in Fig. 1: (a) an outer tail consisting of dusty failed winds (simple up-and-down motions) that resembles the static puffed-up irradiated

disk model of Baskin & Laor (2018) – this component is always present regardless of the adopted values of the initial parameters and for the very low values the full BLR is in this form; (b) an inner region with slightly to largely elongated elliptical orbits; and (c) a funnel-shaped stream of escaping clouds similar to empirical picture of AGNs (Elvis 2000). The last two components may develop (or not) depending on the initial parameters, namely, the black hole mass, accretion rate, and metallicity. As previously discussed but not calculated, it can be expected that the first component may give rise to a double-peaked (disky shape) line profile consistent with observational data for low Eddington sources, however, single-peaked profiles are likely expected from the two latter components (see Naddaf et al. 2021, for more details).

In the previous work, aimed at testing the model, the black hole mass was fixed to $10^8 \, M_\odot$ and we studied the cases with dust-to-gas ratio equivalent to solar metalicity for a range of accretion rates. We did not investigate how changing the black hole mass and other parameters can affect the overall picture. In this paper, we present a large table of results for a relatively wide range of physical parameters of AGNs (introduced in Sect. 3) which we use to test the 2.5D FRADO model, based on calculations of line shapes.

3. Numerical setup

In order to have a relatively broad and comprehensive table of results, the following numerical setup was considered. The main initial physical parameters in this setup, namely, the black hole mass, M_{BH}, dimensionless accretion rate, $\dot{m}$, and dust-to-gas mass ratio Ψ are:

– M_{BH} of $10^6, 10^7, 10^8$, and $10^9 \, M_\odot$.
– $\dot{m}$ of 0.01, 0.1 and 1 in Eddington units defined as:

$$\dot{M}_{edd} = \frac{4\pi G M_{BH} m_p}{\mu \, \sigma_T \, c}, \tag{1}$$

where μ is the accretion efficiency fixed to 0.1. For a reference, the Eddington value for the black hole mass of $10^6 \, M_\odot$ is taken as:

$$\dot{M}_{edd(6)} = 1.399 \times 10^{24} \, [\text{g s}^{-1}]. \tag{2}$$

– Ψ of 0.005 and 0.025, equivalent to one and five times the solar metalicity, respectively.

The first two almost cover the observed range of black hole mass and Eddington rate of AGNs (Shen et al. 2011; Panda et al. 2018). On the other hand, many studies indicate that the metallicity in AGNs can super-solar (see e.g., Hamann & Ferland 1992; Artymowicz et al. 1993; Artymowicz 1993; Matteucci & Padovani 1993; Ferland et al. 1996; Hamann 1997; Warner et al. 2002; Dietrich et al. 2003; Castro et al. 2017; Xu et al. 2018; Shangguan et al. 2018; Sniegowska et al. 2021), even though an observational study by Esparza-Arredondo et al. (2021) has shown that the value of the dust-to-gas ratio for the torus can range from 0.01 to 1 times that of the interstellar medium. Studies also show that there is no correlation between the metallicity in AGNs with either the Eddington rate, black hole mass, or total luminosity (see Du et al. 2014, and references therein). Therefore, in this paper, in addition to the solar value adopted in our previous work, we present our results for five times the solar metallicity, as in Baskin & Laor (2018).

The sublimation temperature of dust is kept at 1500 K (Baskin & Laor 2018) as in Naddaf et al. (2021). The values of

wavelength-dependent dust opacities (as before) are based on the prescriptions of Röllig et al. (2013) and Szczerba et al. (1997) for the classical Mathis–Rumpl–Nordsieck (MRN) dust model (Mathis et al. 1977) consisting of silicate and graphite grains. The standard extended optically thick, geometrically thin disk model of Shakura & Sunyaev (1973) is the source of radiation in our model. As our two previously proposed geometrical configurations for the shielding effect did not show any significant difference, we arbitrarily choose the α-patch model, with an α parameter equal to 3 (as before) for the purposes of consistency (Naddaf et al. 2021).

4. LIL BLR line profiles

The observed line profiles reflect the distribution of the BLR material, velocity field, and local emissivity. In our model, the velocity field is determined, but we still need to provide the amount of material along the trajectories and the efficiency of the line formation at each location. In particular, this last aspect is not simple despite many years of study. Reverberation mapping shows that the lines do respond to the irradiation by the central source, and the formation of LIL lines such as Hβ, MgII, or FeII requires incident hard continuum (far UV). However, the response of the medium to irradiation is complex. The dust radiation pressure alleviating the clouds does not guarantee any line formation in a cloud as long as the cloud does not receive some UV radiation from the central parts. Particularly in the case of LIL lines, the density of the medium is high and, in principle, the collisional excitation, self-shielding, dust content, complex coupling between the continuum and line transfer, and local turbulence should be considered (see e.g., Baldwin 1997; Ilić et al. 2012). Such a comprehensive 3D model is still beyond the scope of the current work.

4.1. Calculation of line profile

Given a distribution of position and velocity of clouds within BLR, we can find the overall shape of line emission by the clouds. On the one hand, the emission wavelengths of clouds are shifted from the rest-frame wavelength depending on their velocity component toward or against the observer due to the relativistic Doppler shift. On the other hand, the position of clouds can provide some weight to the amount of central flux they receive, as well as to their transparency to the observer, namely, the amount of flux re-emitted by each cloud in the form of LIL. The emission from the clouds, depending on their location, might be subject to gravitational redshift as well.

The Doppler shift and gravitational redshift together cause the emitted wavelength λ_{emit} of the cloud line emission to shift toward the observed wavelength λ_{obs}. However, as the radial distance of the onset of LIL BLR from the center is large, of order of several 10^2 (in case of the largest black hole mass and the smallest accretion rate) to a few $10^4 \, r_g$ (in case of the smallest black hole mass and the largest accretion rate), the gravitational redshift is negligible; hence, we only address the Doppler shift here.

In the current paper, we assume a uniform constant cloud density within the entire LIL BLR as the line fitting in LIL BLR (e.g., Adhikari et al. 2016; Panda et al. 2018) supports the universal value for the cloud density. It can be further enhanced in the future by assuming a certain density function for the hot surrounding medium, thus, the pressure balance can yield the density of clouds as a function of the cloud position (Różańska et al. 2006; Baskin & Laor 2018). We do not address

the radiative transfer in our non-hydrodynamic simplified model either.

The most important effect here is that of shielding. In the dynamics, the shielding effect is included which leads to efficient acceleration of the cloud. However, fully shielded clouds do not produce emission lines. When we carry out a posteriori check of clouds that are ultimately well exposed to the central flux, we see that only a small fraction of levitated dust-sublimated clouds in the inner LIL BLR would be directly affected by the central UV radiation. An example of a cloud directly illuminated by the central flux is given and discussed in the section results.

We thus assume that the illumination must be predominantly indirect. This is in agreement with other arguments stating that LIL part of the BLR does not see the full emission from the disk central parts. First argument comes from shorter than expected time delays in higher Eddington ratio sources and it introduces the geometrical concept of two BLR regions – one is closer to the symmetry axis and exposed to irradiation, while the second one is hiding behind the geometrically thick accretion disk (Wang et al. 2014). The other argument comes directly from estimates of the line equivalent width which imply that only a small fraction, namely, on the order of one percent of the nuclear emission, is reprocessed to give the LIL lines such as Hβ, FeII, and the CaII triplet (Panda 2021). We thus assume that this emission must come from the scattering of the central UV radiation.

The presence of highly or fully ionized medium is well supported by observations as well as by the theory. The general picture is nicely illustrated by Ramos Almeida & Ricci (2017), who show the smooth outflow of low density material filling the space between clouds. This medium extends from direct vicinity of a black hole to the narrow line region (NLR) and beyond. In the case of Seyfert 2 galaxies, we see the scattering taking place in the NLR, since the region closer in is still shielded from us, and the reflection reveals the presence of the BLR lines that are otherwise hidden from the observer (Antonucci & Miller 1985). In the case of type 1 sources, we have a clear view down to the nucleus and we see the scatterers all the way down. Closer-in scattering medium consists of hot plasma only. In studies of the polarized light of Seyfert 1 galaxies, these scatterers have been phenomenologically divided into polar and equatorial scatterers (Smith et al. 2004, 2005). However, it well may be a continuous medium, mostly consisting of the innermost fully ionized wind plus intercloud BLR (and further away, also NLR) medium. The amount of such outflows is difficult to estimate, but it has been argued that energy and momentum lead to massive outflows that can be even optically thick for electron scattering (King 2010). The polarization level is rather low, from a fraction of a percent to a few percent (see e.g., Capetti et al. 2021; Popović et al. 2022, for most recent extensive measurements). Such a polarization level is consistent with the optical depth of scatterers on the order of 1, as it largely depends on the viewing angle (Lira et al. 2020). From theoretical point of view, the hot plasma together with the radiation pressure provide the confinement to the clouds (Krolik et al. 1981; Baskin & Laor 2018).

Therefore, the hot medium extending from the black hole vicinity up to BLR distances can scatter a fraction of the nuclear emission towards BLR clouds. Since the temperature of the medium is likely set at a Compton temperature value, $\sim 10^7$ K (Rybicki & Lightman 1986), only Thomson elastic scattering is important. This radiation scattered by the surrounding hot medium reaches to the clouds as illustrated in Fig. 1.

Our previous calculation of column density (Naddaf et al. 2021) indicates that the clouds at higher altitudes are more transparent to the scattered central flux and also to the observer. This motivates us to give some weight to the otherwise uniform intrinsic emissivity of clouds as a function of their vertical position, namely:

$$\epsilon_{\text{tot}} = z \times \epsilon_{\text{int}}, \tag{3}$$

where z is the vertical position of clouds relative to the equatorial plane, and ϵ_{int} is the intrinsic constant emissivity of clouds which we assumed to be uniform throughout the LIL BLR.

As shown in Fig. 1, we assume that in case of formation of stream it may block the ionizing scattered central radiation to reach to outer BLR, so no efficient line emission is expected from that part. In the absence of the stream, lines can be produced by the whole BLR.

It should be noted that in our model, no line emission is expected from the disk itself due to shielding effect. In addition, we do not include any "moon effect" in the line calculations. This moon effect can be the important if the individual clouds are optically thick, so that the illuminated side of the clouds are brighter than the dark side, thus emitting more radiation, (see e.g., Goad et al. 2012; Czerny et al. 2017). Since we have not assumed optically thick clouds in our model, all clouds isotropically emit all the energy they receive (absorb), in the form of line emission. Although the model is symmetric with respect to the equatorial plane, only the clouds above the disk can contribute in the line production as the clouds on the other side are obscured by the disk itself.

4.2. Location of clouds in FRADO

In order to find the distribution of clouds in 2.5D FRADO, we first need to know the number of clouds to be launched at any given radius within the LIL BLR, or equivalently, the disk mass loss rate as a function of radius. The total mass loss rate results directly from our dynamical model (Naddaf et al. 2021), however, in order to have it serve as a function of radius, we adopted a method based on the optically thin approximation in stellar winds. Applying this approach to accretion disk, as in Czerny et al. (2017), yields the following mass loss rate:

$$\dot{M}_z \propto r^{-\frac{5}{2}}. \tag{4}$$

Assuming a constant cloud density, we can then calculate the total number of clouds that we have to launch per given radius in our model. We set the cloud density, arbitrarily and case-specifically, with the aim of obtaining a total number of around two million clouds building the LIL BLR. With the knowledge of the theoretical number of clouds launched at a given radius, a uniform random number generator (URNG) is then used in the following way to provide a non-biased random distribution of clouds. For each cloud launched at a radius, a URNG is used to randomly determine the azimuthal angle at which the cloud should be launched. This is due to that while we do have azimuthal symmetry in our model, we ultimately need a 3D distribution of clouds since the inclined observer breaks the symmetry. We use URNG again for the same launched cloud to find its random position along its trajectory, taking into account the velocity profile along the trajectory.

5. Results

5.1. Trajectories of BLR clouds

Figure 2 displays the trajectories of clouds launched at different radii within LIL BLR for the range of our three main initial physical parameters, namely, black hole mass, accretion rate,
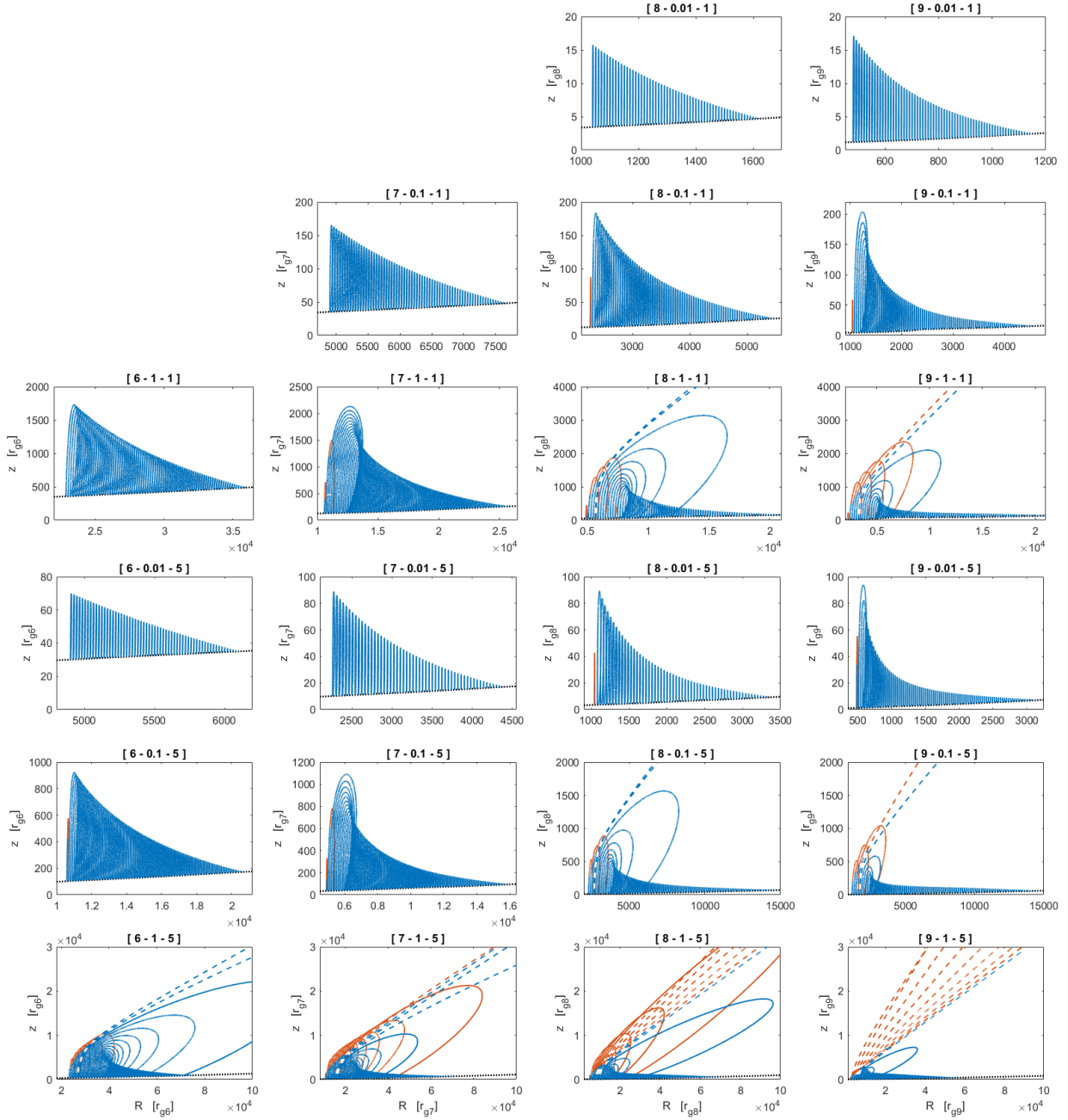
Fig. 2. Trajectories of clouds within BLR in FRADO. The three numbers *from left to right* in brackets atop of each panel stand for log of black hole mass in solar units, accretion rate in Eddington units, and the metallicity in solar units, respectively. The blue and red solid (or dashed) lines show the path of motion of dusty and dustless failed (or escaping) clouds, respectively. The black dotted line represents the disk surface.

and metallicity. The computation of trajectories are done for a very dense equally spaced set of initial radii within the region but only a small fraction of them are plotted for the matter of better visibility. The three blank panels in Fig. 2 indicate that radiation pressure was not efficient enough in those cases to launch any material from the disk.

The results are expressed in terms of black hole mass corresponding gravitational radius defined as:

$$r_{\rm g} = \frac{GM_{\rm BH}}{c^2},\tag{5}$$

which is the minimum for the smallest black hole mass of $10^6 \, M_\odot$ in our sample, that is,

$$r_{\rm g(6)} = 4.78 \times 10^{-8} \, [\text{pc}] = 5.7 \times 10^{-5} \, [\text{lt-day}].\tag{6}$$

As can be seen, the funnel-shaped stream of material can form and get broader with an increase of not only black hole mass and accretion rate, but also with the increase in the dust-to-gas ratio parameter. The stream shows the smallest inclination (relative to the symmetry axis) for the largest values of initial parameters in our model grid, as visible in the bottom-right panel of Fig. 2. The radial extension of BLR, namely, the whole radial range within which a cloud can be lifted from the disk surface also becomes larger with the increase of the values of initial parameters. In our previous study, carried out for the fixed black hole mass of $10^8 \, M_\odot$, we showed that the character of motion in 2.5D FRADO strongly depends on the accretion rate. Now, for the large grid of
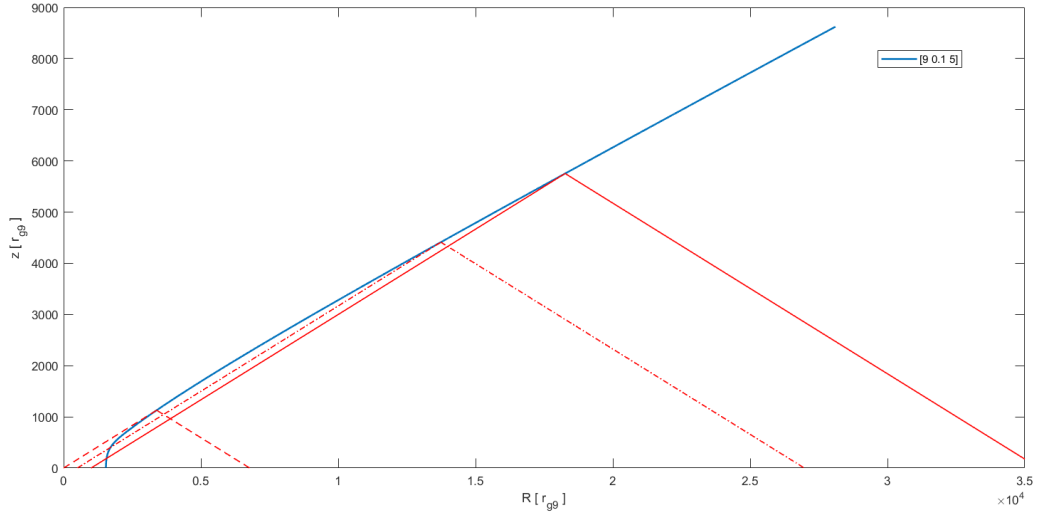
Fig. 3. Illustration of the shielding effect in our model. Here, we show the radial extension of the disk area seen by the selected flying cloud at three different exemplary positions along its trajectory, for the case of escaping cloud launched at $1540\,r_g$ with black hole mass of $10^9\,M_\odot$, Eddington rate of 0.1, and five times solar metallicity. The cloud located at vertical position of around 1100, 4500, and $5800\,r_g$ along its trajectory, sees the radial range of [0–6700], [500–26 800], and [1000–35 600] r_g, respectively. The model assumes the radial visibility as three times higher than the local cloud height ($\alpha = 3$, see Naddaf et al. 2021), so the area at the starting point is very small and we cannot show the early stages in this graphical scale, but the cloud is well exposed to the whole disk irradiation after reaching the height of $1000\,r_g$. Other clouds may never achieve such exposure to the disk central parts.

initial parameters, we can already see that it strongly depends not only on the Eddington rate of the source, but also strongly on the black hole mass and dust-to-gas ratio.

As seen from the results plotted in Fig. 2, there are eight cases in our model grid, each corresponding to a different set of initial parameters, for which the component c (i.e., the outflow stream) is formed. As a result, the component a (i.e., the outer tail) is not expected to contribute in line production as it does not receive the ionizing scattered radiation.

We also provide a scaled illustration of the action of shielding effect in detail in Fig. 3 for the case of an escaping trajectory for a model with black hole mass of $10^9\,M_\odot$, accretion rate of 0.1 in Eddington units, and five times solar metalicity. We illustrate the increasing fraction of the disk visible to the cloud as it moves along the trajectory. This cloud, when reaching a height of around $10^3\,r_g$, is illuminated by the central disk flux. Generally in our model, the clouds for high mass, high accretion rate, and high metallicity can or may be fully directly irradiated when they reach relatively large distances from the center. However, low mass, low Eddington ratio, and low metallicity solutions never predict strong direct exposure of the clouds to full irradiation. In such cases, from the observational point of view, LIL lines do form as well and show the double-peaked profiles, suggesting the line origin to be close to the disk surface, whereas direct irradiation in this case is highly inefficient (see e.g., Loska et al. 2004). This is consistent with the findings from our model.

5.2. Line profiles

Figure 4 shows the full grid of predicted line profiles for the distribution of clumps building the LIL BLR seen at different viewing angles. The line shapes shown in this figure were smoothed with spline technique for better appearance. We set the values of 15, 30, and 45 deg as the representative values for the viewing angle for type 1 AGNs. For these sources, the viewing angle is never very large as the BLR is then obscured by the torus (Antonucci 1993; Netzer 2015).

Consistently with the observations, the lines get narrower with the Eddington ratio (Pounds et al. 1995; Du et al. 2016) of the source and become broader along the black hole mass. Except for the high Eddington rate and high black hole masses, the predicted lines at solar metallicity are dominated by the disk-like shape. However, the higher value of metallicity changes the picture as it allows the efficient rise of material above the disk with vertical velocities comparable to those of the rotational Keplerian one. Generally, an overall view shows that all cases in which the component c of BLR (as shown in Fig. 1) is developed, a single-peaked profile can be expected; other cases without this component give rise to double-peaked line profiles. Comparing the line shapes by eye in terms of the metallicity, we can feasibly argue that the increase of the metallicity by a factor of five corresponds to the increase of the Eddington ratio of the source by a factor of ten. Likewise, we can expect single-peaked profiles for all super-Eddington sources regardless of the black hole mass and metallicity.

There are two important features in the single-peaked predicted profiles: asymmetry and blue-shift. The asymmetry cannot be due to the difference between the time duration of rise and fall of the clouds since in all cases only a very small fraction of failed clouds pass the sublimation location and lose their dust content and continue their motion as a ballistic motion. It means that most clouds complete their full orbit while keeping their dust content so that their motion are not expected to cause line asymmetry. As can be implied from both Figs. 2 and 4, the more intense and broad the outflow stream, the more asymmetric and blue-shifted the line shapes appear. Thus, these two features are interrelated implying that the outflow is dominant compared to the failed part of BLR.

6. Discussion

6.1. Comparison with 1D FRADO

The line shapes predicted by the 2.5D FRADO model show considerable improvement, even approaching characteristic
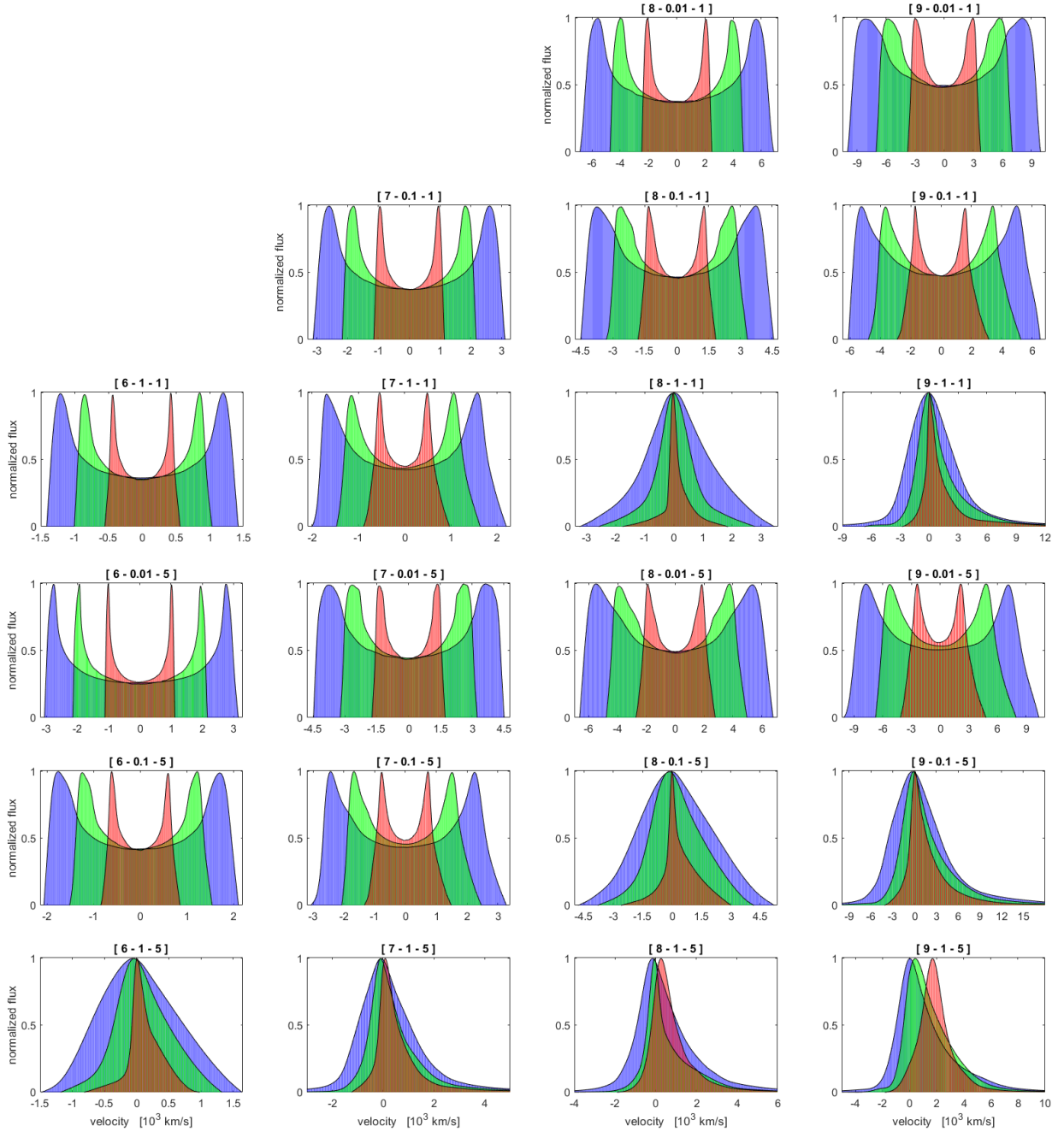
Fig. 4. Predicted dependence of line Profiles (normalized flux to one) on the accretion rate, black hole mass, and dust-to-gas ratio. The numbers in brackets are as in Fig. 2. Lines are color coded with red, green, and blue for the corresponding viewing angles of 15, 30, and 45, respectively.

Lorentzian profiles for high Eddington high black hole mass sources as compared to 1D FRADO, where the double-peaked structure was always obtained (Czerny et al. 2017).

In comparison with the 1D model with constant wavelength-averaged opacities, the 2.5D model is enhanced with the advanced realistic wavelength-dependent values of dust opacities where the dust-to-gas ratio regulates the strength of the radiative force. Increasing the dust-to-gas ratio from a solar value to five times solar (appropriate for quasars as discussed before) leads to a major improvement of the line shape toward single-peaked profiles characteristic for high accretors; whereas this could be obtained in 1D model if the wavelength-averaged dust opacity was greatly increased by a (not entirely realistic) factor of 1000 (Czerny et al. 2017).

6.2. Composite spectrum (mean quasar)

The mean composite quasar spectrum (Vanden Berk et al. 2001) from the Sloan Digital Sky Survey (SDSS) shows that a single-peaked line profile is expected for the LIL BLR. Such a spectrum represents quasars in SDSS data well (Shen et al. 2011), where the mean value of the black hole mass is $10^9 M_\odot$ (Swayamtrupta Panda, priv. comm.), and the mean Eddington ratio is 0.1 (Panda et al. 2018). We thus compared the model, taking the parameters as appropriate for the mean quasar to the MgII and Hβ line shape (shown in Fig. 5). With this aim, we locally subtracted the underlying power-law and then overplotted the theoretical shape of the line assuming arbitrary normalization. In the case of the Hβ line, prior removal of the narrow
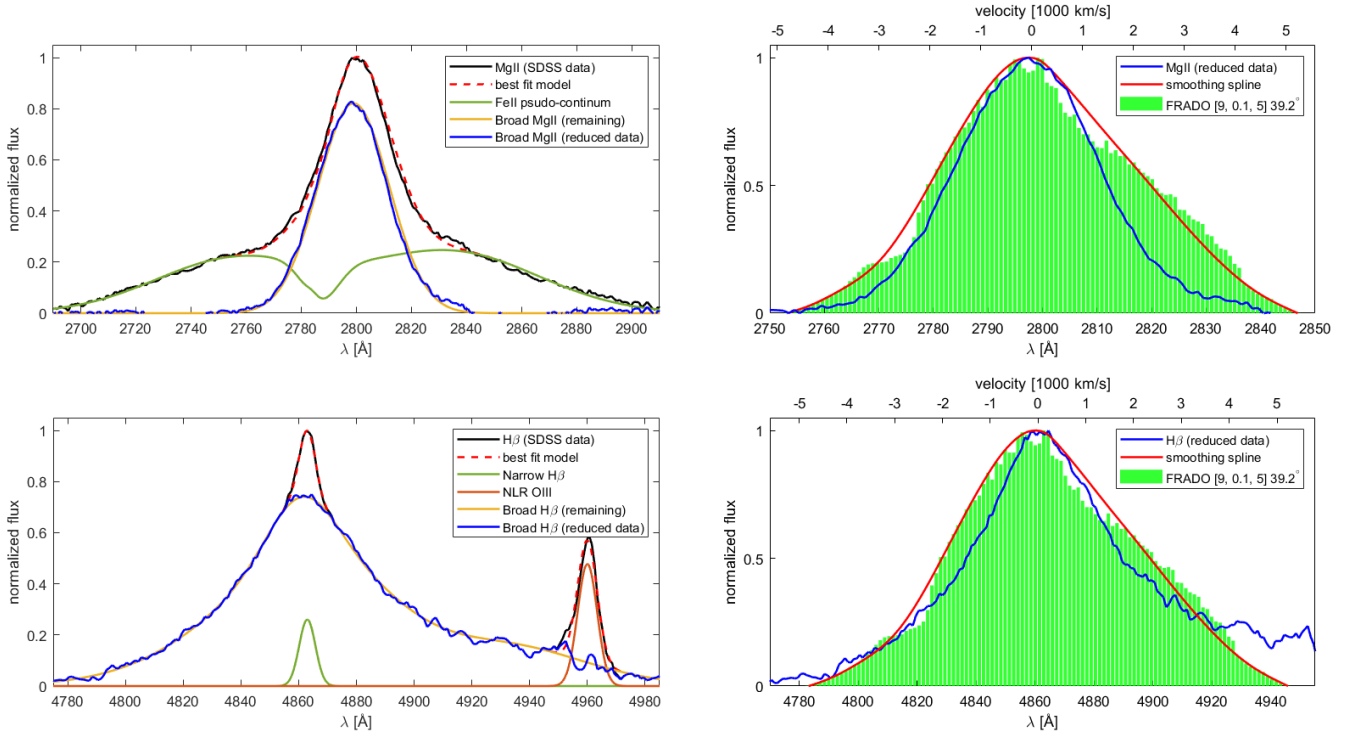
Fig. 5. *Right panels*: comparison of the fully corrected MgII and Hβ lines in the mean composite quasar spectrum from SDSS data to the line profile predicted by 2.5D FRADO for cases corresponding to the mean quasar physical parameters (black hole mass of $10^9 M_\odot$, Eddington rate of 0.1) with metallicity of five times solar, viewed at 30 deg. *Left panels*: power-law-subtracted MgII and Hβ lines from SDSS data are decomposed into different components, as indicated in the plot legends.

Hβ component as well as [OIII] lines coming from the NLR was necessary, and for that we fixed the width of these components at $205\,\mathrm{km\,s^{-1}}$ and $220\,\mathrm{km\,s^{-1}}$ for Hβ and OIII, respectively. As for the MgII line, we used the semi-empirical UV FeII template[1] (Kovačević-Dojčinović & Popović 2015; Popović et al. 2019) to remove the FeII pseudo-continuum in the required spectral band. We see that the results show a nice fit with the data for the LIL part of BLR.

6.3. FWHM vs. σ_{line}

The ratio of the FWHM to the line dispersion, σ_{line}, is an important parameter (Collin et al. 2006) characterizing the line profile, although it does not differentiate between a single and double-peaked profiles. We calculated this ratio for the grid of our initial physical parameters (with Fig. 6 displaying the results). Most models are roughly consistent with the ratio expected for a Gaussian, but for high-mass, high-Eddington ratio models, this ratio dropped considerably, indicating that we are approaching Lorentzian profiles. Therefore, although the Lorentzian profiles might simply be expected for extremely low viewing angles (e.g., Goad et al. 2012), our results show that sources with high mass high Eddington ratio can generally lead to relatively Lorentzian shapes, regardless of the viewing angle. Moreover, the larger the black hole mass and accretion rate are, the more asymmetry and blue-shift in the line shape we have, as shown in Fig. 4.

This trend is overall consistent with the data (see e.g., Marziani et al. 2003). The strong trend with the change of the viewing angle is visible for high Eddington sources, whereas for the remaining sources, the effect is weak when FWHM/σ_{line}

---

[1] http://servo.aob.rs/FeII_AGN/link7.html

is used. What is somewhat surprising is the very strong trend related to the black hole mass, which is also visible in Fig. 4.

6.4. Model assumptions

In our model, we used a non-hydrodynamical approach based on assumptions of the motion of separate clouds under gravity and the action of radiation pressure acting on dust. This has considerable limitations but they are justified as the first approximation for modeling the LIL part of the BLR. As discussed in the classical paper of line-driven wind model (for HIL part of BLR) by Murray et al. (1995), the optical depth of the emitting region must be moderate (column density of order of $10^{23}\,\mathrm{cm^{-2}}$) and the local density is high (for LIL part it is higher than that of HIL, many authors argue for a local density about $10^{12}\,\mathrm{cm^{-3}}$, for instance, Adhikari et al. 2016; Baskin & Laor 2018; Panda et al. 2018), while the BLR is extended. There are two possibilities to support a consistent picture: it is either to assume a very narrow stream of material flowing out, with the cross-section on the order of $10^{12}\,\mathrm{cm}$, as in Murray et al. (1995), where they assume lower density so the size is actually larger $10^{14}\,\mathrm{cm}$; or to assume considerable clumpiness of the medium. We followed the second approach since there are natural thermal instabilities in the plasma, such as instability caused by X-ray irradiation (Krolik et al. 1981). In this case, the plasma spontaneously forms colder clumps (at a temperature of $\sim 10^4$ K, cooled through atomic processes) embedded in a hotter medium (at temperature $\sim 10^7$ K, set at an inverse Compton temperature value). The presence of highly or fully ionized medium is aptly supported by the observations as well as by the theory. Then the two media of density contrast of order of 10^3 provide the rough pressure balance. Blandford et al. (1990) discussed the typical values for
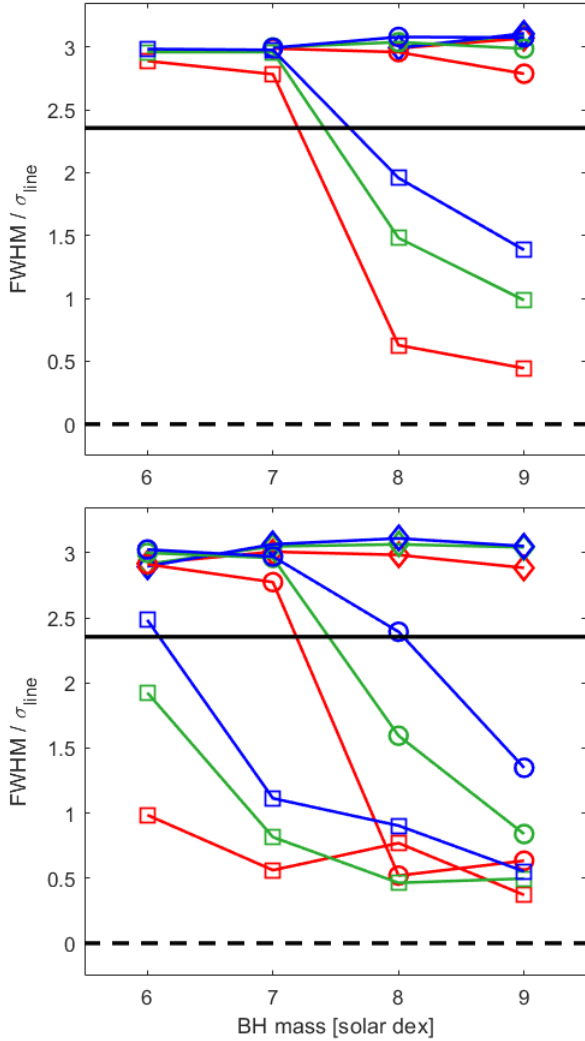
Fig. 6. Dependence of the ratio of FWHM/σ_{line} on the initial physical parameters for the solar (*upper panel*) and five times solar metallicity (*lower panel*). The red, green, and blue solid lines represents the viewing angles of 15, 30, and 45 deg, respectively. The diamonds, circles, and squares stand for the Eddington rates of 0.01, 0.1, and 1, respectively. The values of 2.3548 and zero expected for a Gaussian and Lorentzian profile are depicted by black solid and black dashed lines, respectively, for a reference.

ionization parameter in AGN clouds covering the range from 10^{-3} to 1, that is, up to four orders of magnitudes. The precise description of the structure of the clumpy medium is very difficult. Even in the case of a single cloud exposed to irradiation, in plane-parallel approximation requires a radiative transfer to be performed, which would then show the gradual change in the density, temperature, and ionization parameters (see e.g., Baskin & Laor 2018; Adhikari et al. 2018), with the low density first and the temperature roughly at inverse Compton temperature (depending on the shape of the incident spectrum), and then a relatively rapid decrease at the subsequent ionization fronts. A proper description of this transition, calculated under constant pressure, actually requires inclusion of the electron conduction (e.g., Begelman & McKee 1990; Różańska & Czerny 2000). Deep within the cloud, there is a further drop in temperature and a rise in density due to a decrease in the local flux as a result of absorption. As emphasized by Baskin & Laor (2018), radiation pressure also plays a dynamical role in this pro-

cess. The picture is further complicated if plane-parallel approximation is abandoned. The presence of the numerous clouds of complex shapes can be fully consistent with simple estimates of the cloud number based on line shape properties as done by Arav et al. (1998). Of course, there are also certain processes that can lead to cloud destruction, such as the action of tidal forces (Müller et al. 2022), Kelvin–Helmholtz instabilities, and cloud ablation), however, the destruction rate can be strongly affected by the magnetic field (e.g., McCourt et al. 2015). The relative importance between the condensation rate and destruction rate depends on the cloud size, as it is set roughly by the field length (Field 1965). Cloud formation in AGN has been seen in the numerical simulations from Waters et al. (2021), but at distances much greater than the BLR distance which was likely related to the numerical setup and the requested spatial resolution of the computations. The issue is thus extremely complex, and simple order-of-magnitude estimates based on a single density and single temperature of the cloud and intercloud medium are not fully adequate and cannot reproduce the full ionization parameter range. However, addressing this point in detail is beyond the scope of the current paper.

Our model contains one more important simplification. We assumed only the action of the radiation pressure acting on the dust, and we neglect the line driving effect. Close to the launching point, the local flux comes from the disk, without any considerable UV component, but when the clouds is alleviated high above the disk, the line-driving effect should set in. There have been numerous papers addressing the line-driven winds (Murray et al. 1995; Proga et al. 2000; Risaliti & Elvis 2010; see Giustini et al. 2020 for a recent review) but none of the studies have combined dust radiation pressure and line pressure in this context since the way of determining the radiative force is very different in these two scenarios. Our negligence of the line driving is most likely appropriate for description of launching clouds at the LIL BLR, but it underestimated the cloud velocities when the outflowing stream of the material forms. This effect should be incorporated in the future studies; specifically, we should combine our code with the QWIND (Risaliti & Elvis 2010; Quera-Bofarull et al. 2021) but this is not easy even in the case of non-hydrodynamical simulations.

The expected higher velocities of the clouds due to line driving will partially be slowed down by the interaction of the clouds with the ambient medium, which is also neglected in our model. The freshly launched clouds and inter-cloud medium are co-moving since clouds form through thermal instability. However, accelerating clouds detach from their surrounding and, thereby, some drag force is expected, although clouds are much denser than the ambient medium (roughly in pressure equilibrium) and the relative velocities between the hot medium and the clouds are not very high. This is because clouds and the intercloud medium likely share the Keplerian motion component of the velocity and follow the same initial vertical velocity gained before the fragmentation of the medium into clouds occurred.

Wind models having elements of the radiative transfer show single-peaked lines (Murray et al. 1995; Waters et al. 2016). In our work, with a simplified non-hydrodynamic approach to the dynamics of material in LIL BLR, the single-peaked profiles are obtained without incorporating the process of radiative transfer into the emissivity of clouds.

In a future work, it will be necessary to address the issue of cloud emissivity in more detail, including line formation in the dusty medium. However, this effect is strongly dependent not only on cloud irradiation but also on cloud local densities. At low densities, the presence of dust suppresses line

emission (Netzer & Laor 1993), while at high densities (above $10^{11.5}$ cm^{-3}), emission lines do form efficiently even in the presence of the dust. This explains the absence of a gap between the NLR and BLR region in narrow-line Seyfert 1 galaxies (Adhikari et al. 2016).

The assumption of the dust sublimation temperature fixed in the at 1500 K is simple to relax, and higher (or lower) temperature will predominantly shift the position of the BLR outward (or inward). This will be important for precise comparison of the radius–luminosity relation to the observational data, but we do not yet focus on this goal here. Indeed, a higher average temperature of ~1700 K is quite likely, but 1500 K is still frequently assumed even in data analysis (e.g., GRAVITY Collaboration 2020b) and broadband spectral fitting of the dust emission in AGN gives the values in individual sources in the range of 1000–1750 K (Hernán-Caballero et al. 2016). The more advanced approach, taking into account the specific dust species, like silicates, amorphous carbon, and so on, and the dependence of the sublimation temperature not only on the chemical composition, but also on specific grain size is far more complicated since the loss of the driving pressure force would be gradual, and the dust composition would have to be recalculated at each integration step for each cloud trajectory. This should be done at some stage, but a number of simplifications still used to recover the dynamics and the line emissivity do not yet require such an advanced approach.

7. Summary

Following our previous work on the dynamical character and shape of LIL BLR based on the non-hydrodynamic single-cloud 2.5D FRADO model (Naddaf et al. 2021), we here tested the model by calculation of line profiles for the model-concluded distribution of clouds along their trajectories within LIL BLR, for a relatively large grid of initial conditions. We adopted a simple approach, assuming a constant cloud density and without the element of radiative transfer included.

The predicted trend in the line shape seems consistent with observations, as the model implies narrower (or broader) line shape for sources with larger Eddington ratio (or smaller black hole mass). All solutions with a developed outflow stream of material show up single-peaked profiles, and the line shape approaches a Lorentzian shape for a high-mass high Eddington ratio. In other cases, a double-peaked disk-like line shape dominates.

Two features, namely: asymmetry and blue-shifting, seen in the line shapes developed in the cases with outflow streams show that the outflow is dominant compared to failed trajectories. These features were more visibly intense for the sources with high black hole mass and high Eddington ratios. Most importantly, we showed that the line profile predicted by our model for the case with initial physical parameters corresponding to those of the mean quasar is consistent with observed mean spectrum seen in the SDSS composite.

References

Adhikari, T. P., Różańska, A., Czerny, B., Hryniewicz, K., & Ferland, G. J. 2016, ApJ, 831, 68
Adhikari, T. P., Hryniewicz, K., Różańska, A., Czerny, B., & Ferland, G. J. 2018, ApJ, 856, 78
Antonucci, R. 1993, ARA&A, 31, 473
Antonucci, R. R. J., & Miller, J. S. 1985, ApJ, 297, 621
Arav, N., Barlow, T. A., Laor, A., Sargent, W. L. W., & Blandford, R. D. 1998, MNRAS, 297, 990
Artymowicz, P. 1993, PASP, 105, 1032
Artymowicz, P., Lin, D. N. C., & Wampler, E. J. 1993, ApJ, 409, 592
Baldwin, J. A. 1997, in IAU Colloq. 159: Emission Lines in Active Galaxies: New Methods and Techniques, eds. B. M. Peterson, F. Z. Cheng, & A. S. Wilson, ASP Conf. Ser., 113, 80
Baskin, A., & Laor, A. 2018, MNRAS, 474, 1970
Begelman, M. C., & McKee, C. F. 1990, ApJ, 358, 375
Bentz, M. C., Walsh, J. L., Barth, A. J., et al. 2009, ApJ, 705, 199
Bentz, M. C., Denney, K. D., Grier, C. J., et al. 2013, ApJ, 767, 149
Blandford, R. D., & McKee, C. F. 1982, ApJ, 255, 419
Blandford, R. D., Netzer, H., Woltjer, L., Courvoisier, T. J. L., & Mayor, M. 1990, Active Galactic Nuclei (Berlin: Springer-Verlag)
Boroson, T. A., & Green, R. F. 1992, ApJS, 80, 109
Capetti, A., Laor, A., Baldi, R. D., Robinson, A., & Marconi, A. 2021, MNRAS, 502, 5086
Castro, C. S., Dors, O. L., Cardaci, M. V., & Hägele, G. F. 2017, MNRAS, 467, 1507
Collin-Souffrin, S., Dyson, J. E., McDowell, J. C., & Perry, J. J. 1988, MNRAS, 232, 539
Collin, S., Kawaguchi, T., Peterson, B. M., & Vestergaard, M. 2006, A&A, 456, 75
Czerny, B., & Hryniewicz, K. 2011, A&A, 525, L8
Czerny, B., Du, P., Wang, J.-M., & Karas, V. 2016, ApJ, 832, 15
Czerny, B., Li, Y.-R., Hryniewicz, K., et al. 2017, ApJ, 846, 154
Dietrich, M., Hamann, F., Shields, J. C., et al. 2003, ApJ, 589, 722
Dong, X., Wang, T., Wang, J., et al. 2008, MNRAS, 383, 581
Du, P., Wang, J.-M., Hu, C., et al. 2014, MNRAS, 438, 2828
Du, P., Lu, K.-X., Zhang, Z.-X., et al. 2016, ApJ, 825, 126
Dyda, S., & Proga, D. 2018, MNRAS, 475, 3786
Elvis, M. 2000, ApJ, 545, 63
Esparza-Arredondo, D., Gonzalez-Martín, O., Dultzin, D., et al. 2021, A&A, 651, A91
Ferland, G. J., Baldwin, J. A., Korista, K. T., et al. 1996, ApJ, 461, 683
Field, G. B. 1965, ApJ, 142, 531
Ganguly, S., Proga, D., Waters, T., et al. 2021, ApJ, 914, 114
Gaskell, C. M. 2009, New Astron. Rev., 53, 140
Gezari, S., Halpern, J. P., & Eracleous, M. 2007, ApJS, 169, 167
Giustini, M., & Proga, D. 2020, in Nuclear Activity in Galaxies Across Cosmic Time, eds. M. Pović, P. Marziani, J. Masegosa, et al., 356, 82
Goad, M. R., Korista, K. T., & Ruff, A. J. 2012, MNRAS, 426, 3086
GRAVITY Collaboration (Sturm, E., et al.) 2018, Nature, 563, 657
GRAVITY Collaboration (Amorim, A., et al.) 2020a, A&A, 643, A154
GRAVITY Collaboration (Dexter, J., et al.) 2020b, A&A, 635, A92
GRAVITY Collaboration (Amorim, A., et al.) 2021, A&A, 648, A117
Grier, C. J., Peterson, B. M., Horne, K., et al. 2013, ApJ, 764, 47
Guerras, E., Mediavilla, E., Jimenez-Vicente, J., et al. 2013, ApJ, 764, 160
Hamann, F. 1997, ApJS, 109, 279
Hamann, F., & Ferland, G. 1992, ApJ, 391, L53
Hernán-Caballero, A., Hatziminaoglou, E., Alonso-Herrero, A., & Mateos, S. 2016, MNRAS, 463, 2064
Horne, K., Welsh, W. F., & Peterson, B. M. 1991, ApJ, 367, L5
Ilić, D., Popović, L. Č., La Mura, G., Ciroi, S., & Rafanelli, P. 2012, A&A, 543, A142
Kaspi, S., Smith, P. S., Netzer, H., et al. 2000, ApJ, 533, 631
King, A. R. 2010, MNRAS, 402, 1516
Kovačević-Dojčinović, J., & Popović, L. Č. 2015, ApJS, 221, 35
Krolik, J. H., & Done, C. 1995, ApJ, 440, 166
Krolik, J. H., McKee, C. F., & Tarter, C. B. 1981, ApJ, 249, 422
Lawrence, A., Elvis, M., Wilkes, B. J., McHardy, I., & Brandt, N. 1997, MNRAS, 285, 879
Le, H. A. N., & Woo, J.-H. 2019, ApJ, 887, 236
Li, Y.-R., Wang, J.-M., Ho, L. C., Du, P., & Bai, J.-M. 2013, ApJ, 779, 110
Li, Y.-R., Wang, J.-M., & Bai, J.-M. 2016, ApJ, 831, 206
Li, S.-S., Yang, S., Yang, Z.-X., et al. 2021, ApJ, 920, 9
Lira, P., Goosmann, R. W., Kishimoto, M., & Cartier, R. 2020, MNRAS, 491, 1
Loska, Z., Czerny, B., & Szczerba, R. 2004, MNRAS, 355, 1080
Lu, K.-X., Wang, J.-G., Zhang, Z.-X., et al. 2021, ApJ, 918, 50
Marziani, P., Sulentic, J. W., Zamanov, R., et al. 2003, ApJS, 145, 199
Mathis, J. S., Rumpl, W., & Nordsieck, K. H. 1977, ApJ, 217, 425
Matteucci, F., & Padovani, P. 1993, ApJ, 419, 485
McCourt, M., O'Leary, R. M., Madigan, A.-M., & Quataert, E. 2015, MNRAS, 449, 2
Mizumoto, M., Done, C., Tomaru, R., & Edwards, I. 2019, MNRAS, 489, 1152
Müller, A.L., Naddaf, M.H., Zajaček, M., et al. 2022, ApJ, 931, 39

Murray, N., Chiang, J., Grossman, S. A., & Voit, G. M. 1995, ApJ, 451, 498
Naddaf, M.-H., Czerny, B., & Szczerba, R. 2020, Front. Astron. Space Sci., 7, 15
Naddaf, M.-H., Czerny, B., & Szczerba, R. 2021, ApJ, 920, 30
Negrete, C. A., Dultzin, D., Marziani, P., et al. 2018, A&A, 620, A118
Netzer, H. 2013, The Physics and Evolution of Active Galactic Nuclei (Cambridge: Cambridge University Press)
Netzer, H. 2015, ARA&A, 53, 365
Netzer, H. 2020, MNRAS, 494, 1611
Netzer, H., & Laor, A. 1993, ApJ, 404, L51
Osterbrock, D. E. 1977, ApJ, 215, 733
Osterbrock, D. E. 1981, ApJ, 249, 462
Pancoast, A., Brewer, B. J., & Treu, T. 2011, ApJ, 730, 139
Pancoast, A., Brewer, B. J., & Treu, T. 2014, MNRAS, 445, 3055
Panda, S. 2021, A&A, 650, A154
Panda, S., Czerny, B., Adhikari, T. P., et al. 2018, ApJ, 866, 115
Peterson, B. M., Ferrarese, L., Gilbert, K. M., et al. 2004, ApJ, 613, 682
Popović, L. Č., Kovačević-Dojčinović, J., & Marčeta-Mandić, S. 2019, MNRAS, 484, 3180
Popović, L. Č., Shablovinskaya, E., & Savić, D. 2022, Astron. Nachr., 343, e210089
Pounds, K. A., Done, C., & Osborne, J. P. 1995, MNRAS, 277, L5
Proga, D., & Kallman, T. R. 2004, ApJ, 616, 688
Proga, D., Stone, J. M., & Kallman, T. R. 2000, ApJ, 543, 686
Quera-Bofarull, A., Done, C., Lacey, C. G., Nomura, M., & Ohsuga, K. 2021, ArXiv e-prints [arXiv:2111.02742]
Raimundo, S. I., Vestergaard, M., Goad, M. R., et al. 2020, MNRAS, 493, 1227
Ramos Almeida, C., & Ricci, C. 2017, Nat. Astron., 1, 679
Rees, M. J., Silk, J. I., Werner, M. W., & Wickramasinghe, N. C. 1969, Nature, 223, 788
Reeves, J. N., & Turner, M. J. L. 2000, MNRAS, 316, 234
Risaliti, G., & Elvis, M. 2010, A&A, 516, A89
Röllig, M., Szczerba, R., Ossenkopf, V., & Glück, C. 2013, A&A, 549, A85
Różańska, A., & Czerny, B. 2000, MNRAS, 316, 473
Różańska, A., Czerny, B., Życki, P. T., & Pojmański, G. 1999, MNRAS, 305, 481
Różańska, A., Goosmann, R., Dumont, A. M., & Czerny, B. 2006, A&A, 452, 1
Rybicki, G. B., & Lightman, A. P. 1986, Radiative Processes in Astrophysics (Germany: Wiley-VCH)
Shakura, N. I., & Sunyaev, R. A. 1973, A&A, 500, 33
Shangguan, J., Ho, L. C., & Xie, Y. 2018, ApJ, 854, 158
Shen, Y., Richards, G. T., Strauss, M. A., et al. 2011, ApJs, 194, 45
Shlosman, I., Vitello, P. A., & Shaviv, G. 1985, ApJ, 294, 96
Sluse, D., Hutsemékers, D., Courbin, F., Meylan, G., & Wambsganss, J. 2012, A&A, 544, A62
Smith, J. E., Robinson, A., Alexander, D. M., et al. 2004, MNRAS, 350, 140
Smith, J. E., Robinson, A., Young, S., Axon, D. J., & Corbett, E. A. 2005, MNRAS, 359, 846
Ṡniegowska, M., Marziani, P., Czerny, B., et al. 2021, ApJ, 910, 115
Sulentic, J. W., Marziani, P., & Dultzin-Hacyan, D. 2000, ARA&A, 38, 521
Szczerba, R., Omont, A., Volk, K., Cox, P., & Kwok, S. 1997, A&A, 317, 859
Vanden Berk, D. E., Richards, G. T., Bauer, A., et al. 2001, AJ, 122, 549
Voit, G. M. 1992, MNRAS, 258, 841
Wandel, A., Peterson, B. M., & Malkan, M. A. 1999, ApJ, 526, 579
Wang, J.-M., Qiu, J., Du, P., & Ho, L. C. 2014, ApJ, 797, 65
Ward, R. L., Wadsley, J., & Sills, A. 2014, MNRAS, 445, 1575
Warner, C., Hamann, F., Shields, J. C., et al. 2002, ApJ, 567, 68
Waters, T., Kashi, A., Proga, D., et al. 2016, ApJ, 827, 53
Waters, T., Proga, D., & Dannen, R. 2021, ApJ, 914, 62
Xu, F., Bian, F., Shen, Y., et al. 2018, MNRAS, 480, 345
Zhang, Z.-X., Du, P., Smith, P. S., et al. 2019, ApJ, 876, 49